Electronic Supplementary Information

Unveiling the Photocatalytic Potential of Two-Dimensional Ferroelastic LuSX Monolayers for Efficient Water Splitting: A First-Principles Discovery

Fengxian Ma,[a] Xiaoxia Liu,[a] Zhen Gao, [a] Zibo Chen, [a] Yalong Jiao,[a,*]
Zhongfang Chen[b,*]

[a] College of Physics, Hebei Key Laboratory of Photophysics Research and Application, Hebei Normal University, Shijiazhuang 050024, China.
[b] Department of Chemistry, University of Puerto Rico, Rio Piedras Campus, San Juan, PR 00931, USA.

*E-mail:
yalong.jiao@hebtu.edu.cn; zhongfang.chen1@upr.edu

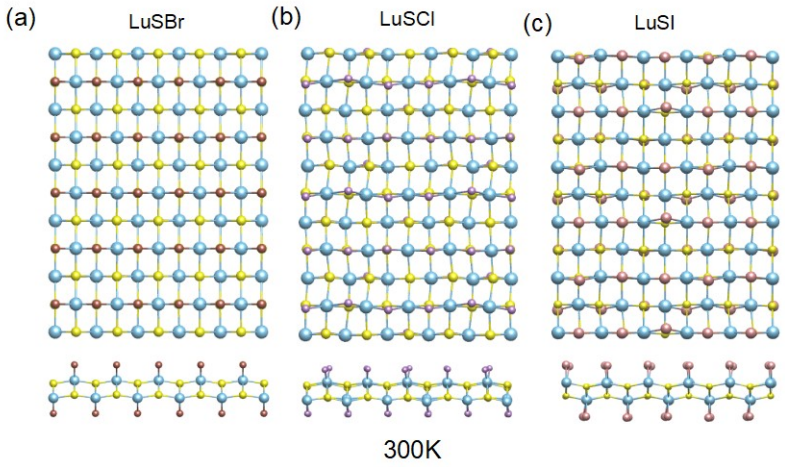

Fig. S1. AIMD snapshots of (a) LuSBr, (b) LuSCl, and (c) LuSI monolayer at 300 K.

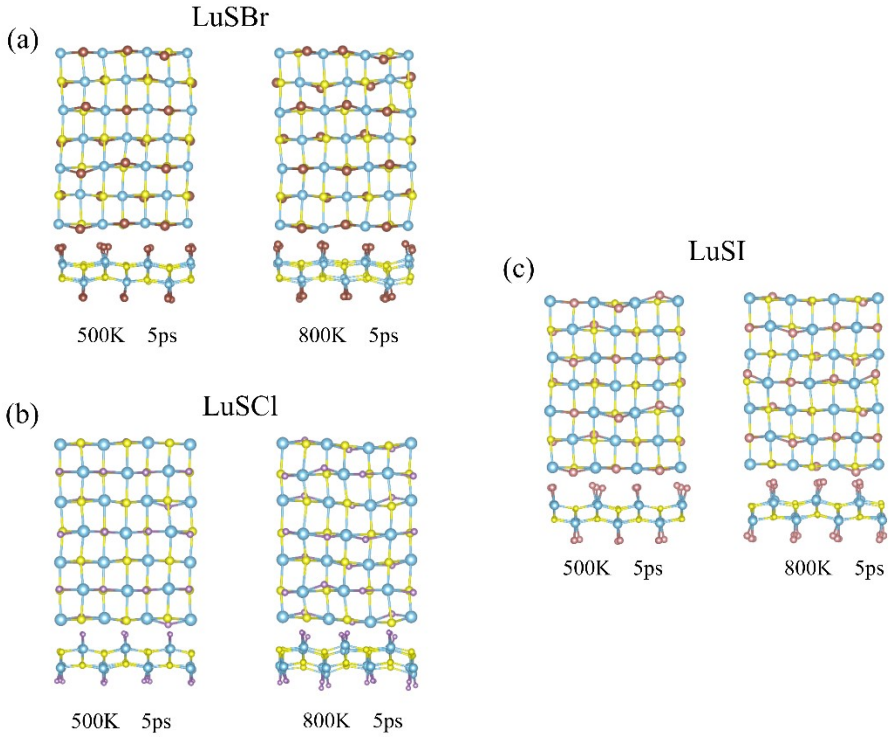

Fig. S2. AIMD snapshots of (a) LuSBr, (b) LuSCl, and (c) LuSI monolayer at 500 K and 800 K.

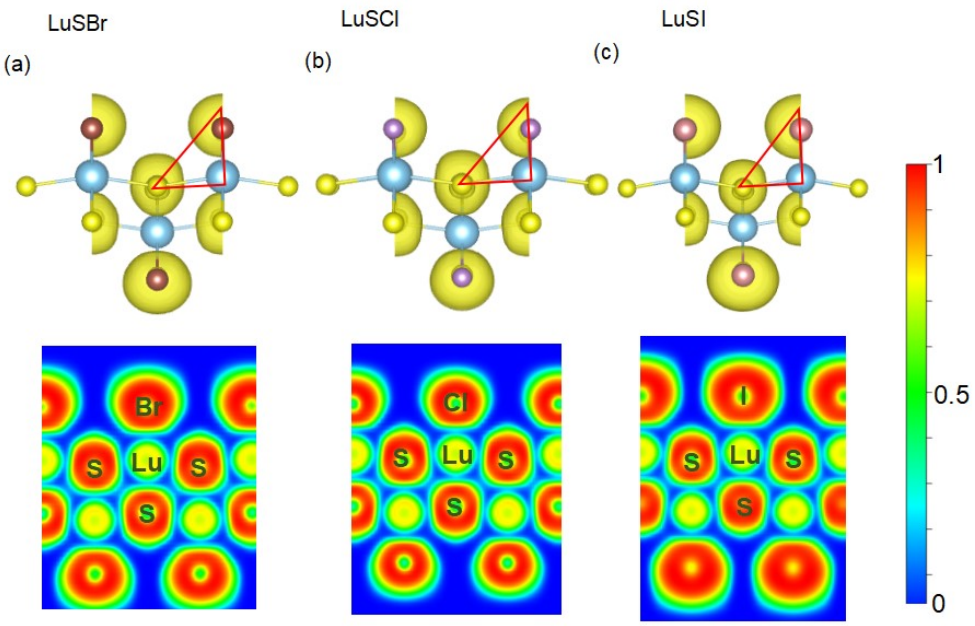

Fig. S3. (a-c) Side views and corresponding electron localization function (ELF) contour maps cut along the (001) direction, with equivalent values of 0.9au, 0.89au., and 0.9au, respectively. The red line represents the selected layer shown in the ELF contour map in the bottom panel.

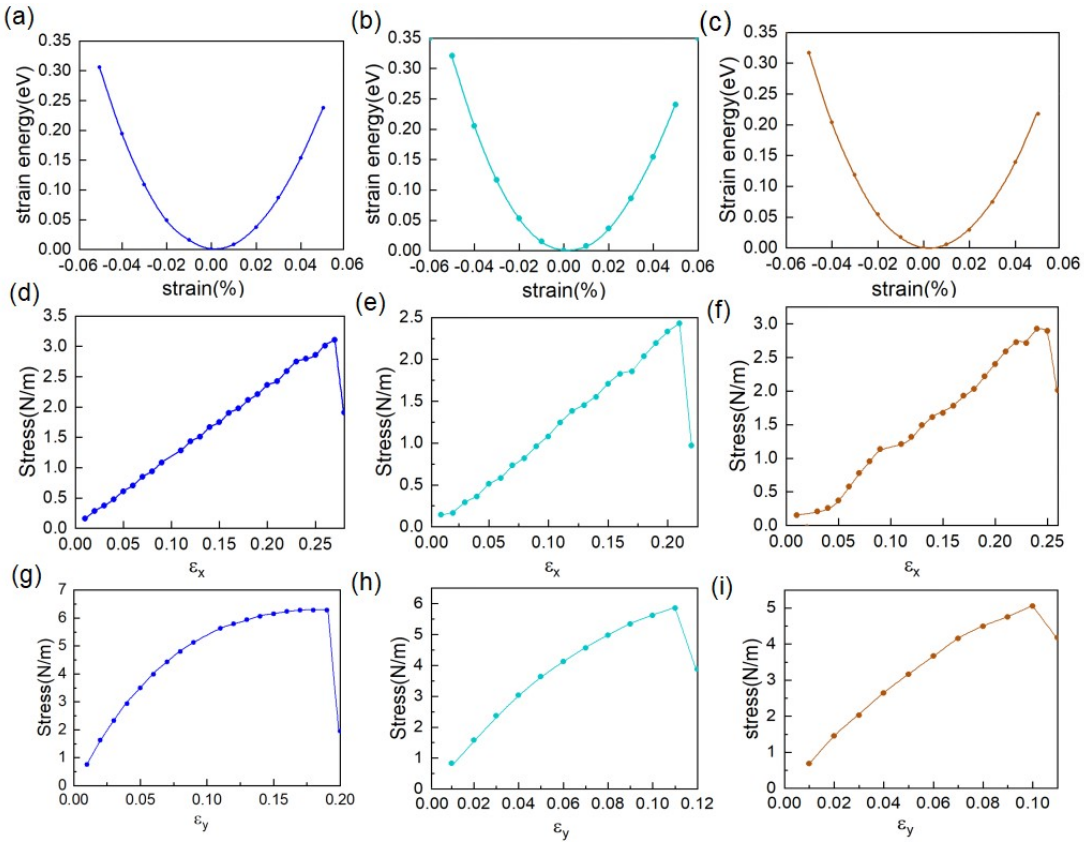

Fig. S4. (a-c) Total energy variation of LuSBr, LuSCl, and LuSI monolayers under biaxial strain ranging from -5% to 5%. (d-f) Stress-strain curves for the three layers under strain along the *x* direction. (g-i) Stress-strain curves for the three layers under strain along the *y* direction.

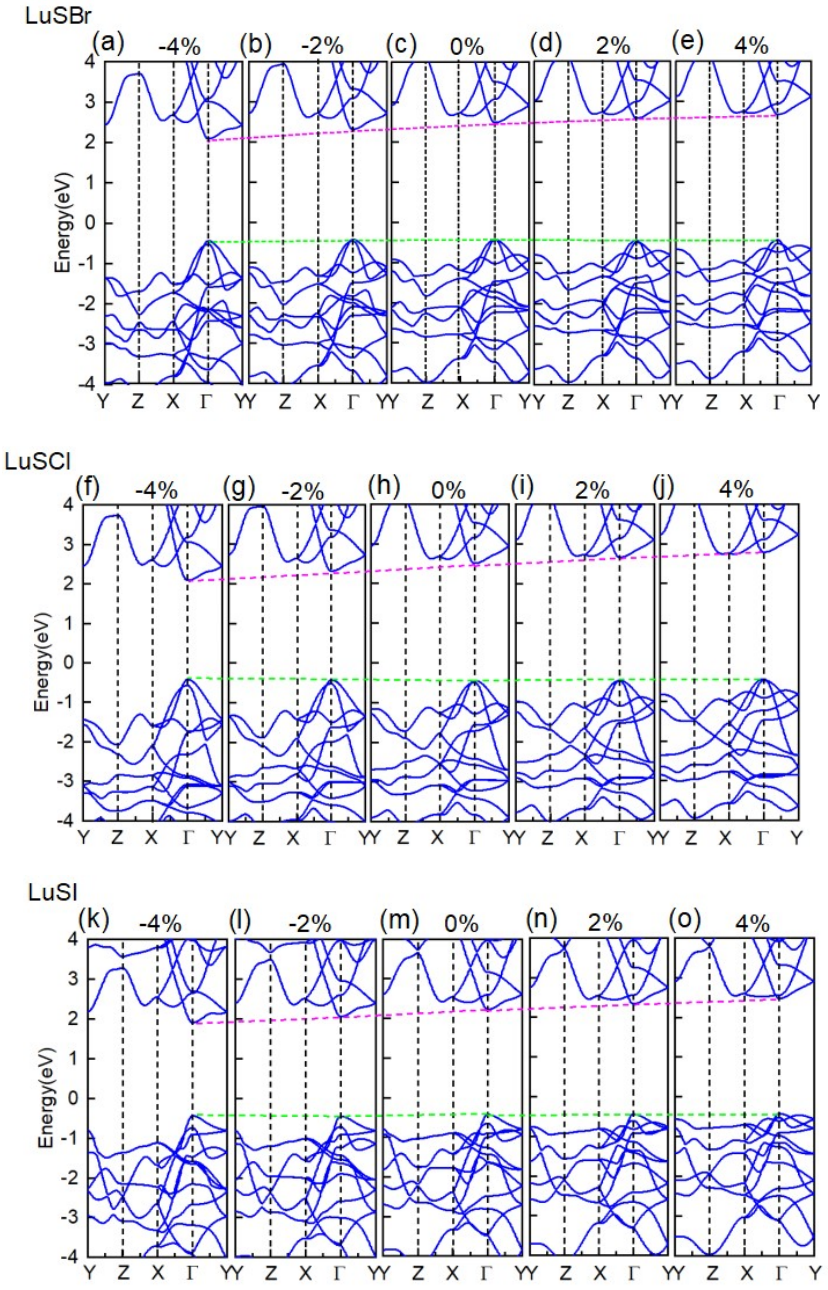

Fig. S5. Band structures of LuSBr, LuSCl, and LuSI monolayers under external strains.

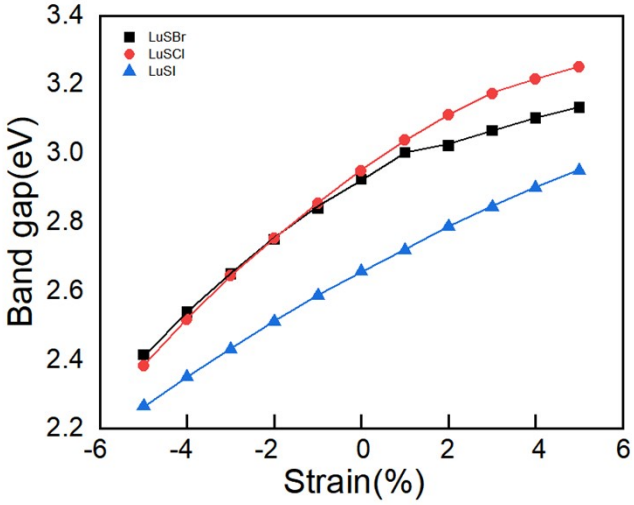

Fig. S6. Variation in band gap values of the LuSX monolayer under in-plane biaxial strain ranging from -5% to 5%.

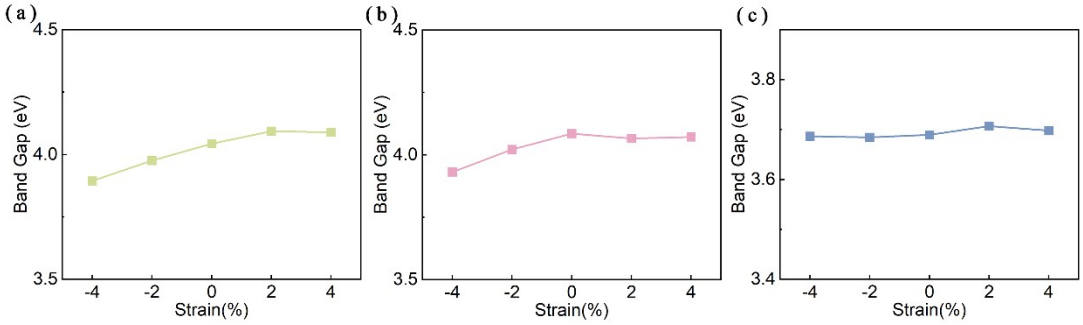

Fig. S7. The variation of band gaps for (a) LuSBr, (b) LuSCl, and (c) LuSI sheets under uniaxial strains.

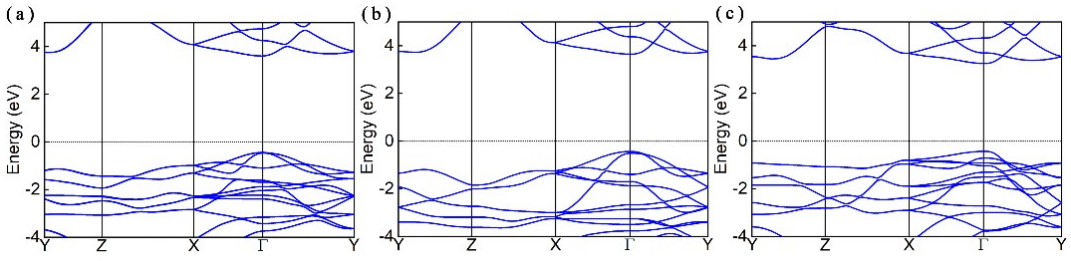

Fig. S8. (a-c) Band structures of the F' state of LuSBr, LuSCl, LuSI sheets.

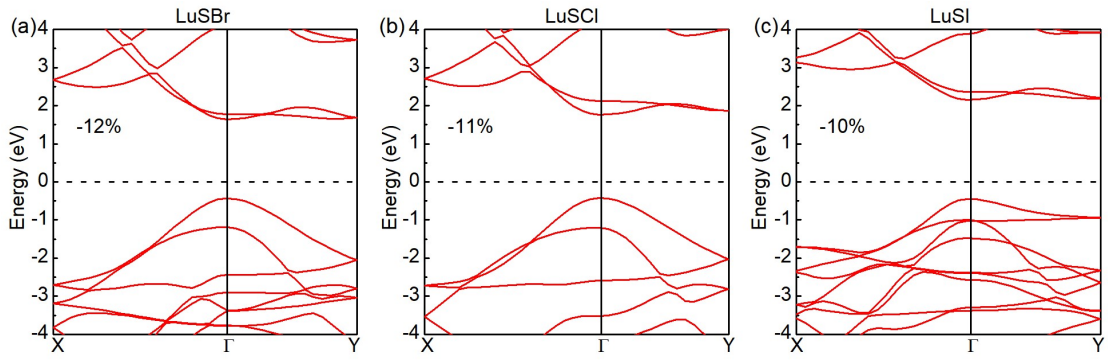

Fig. S9. Band structures of (a) LuSBr, (b) LuSCl, and (c) LuSI monolayers with the strain of -12%, -11%, and -10%, respectively.

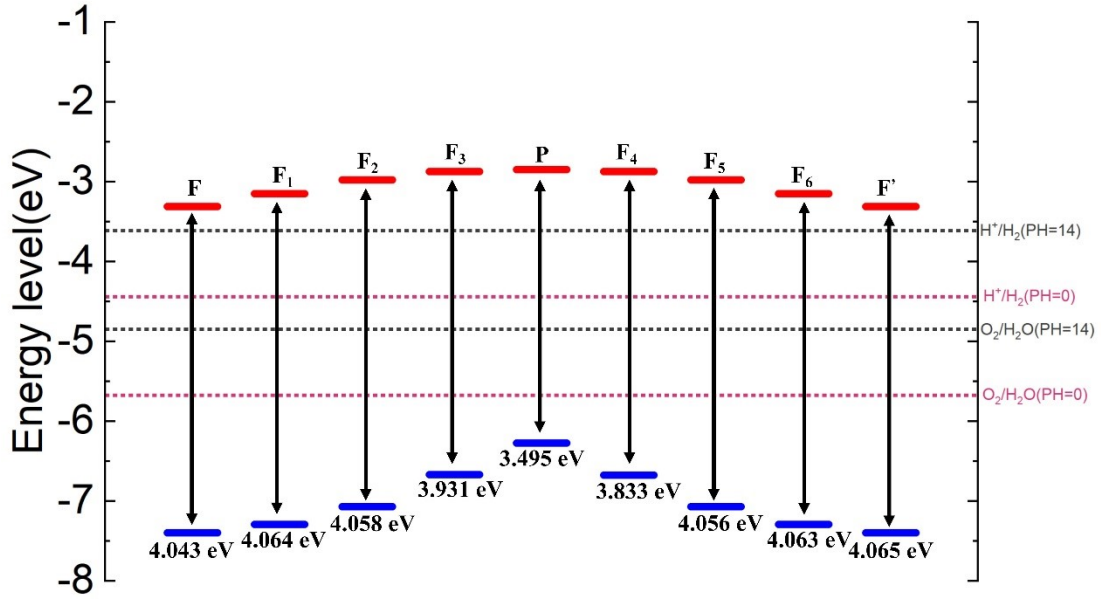

Fig. S10. Band-edge positions of different states of LuSBr monolayer during FE switching, shown in relation to the redox potentials of water, calculated using the HSE06 functional. The vacuum energy level is set to 0 eV. Intermediate states labeled F1 to F6 correspond to those identified in Fig. 4d.

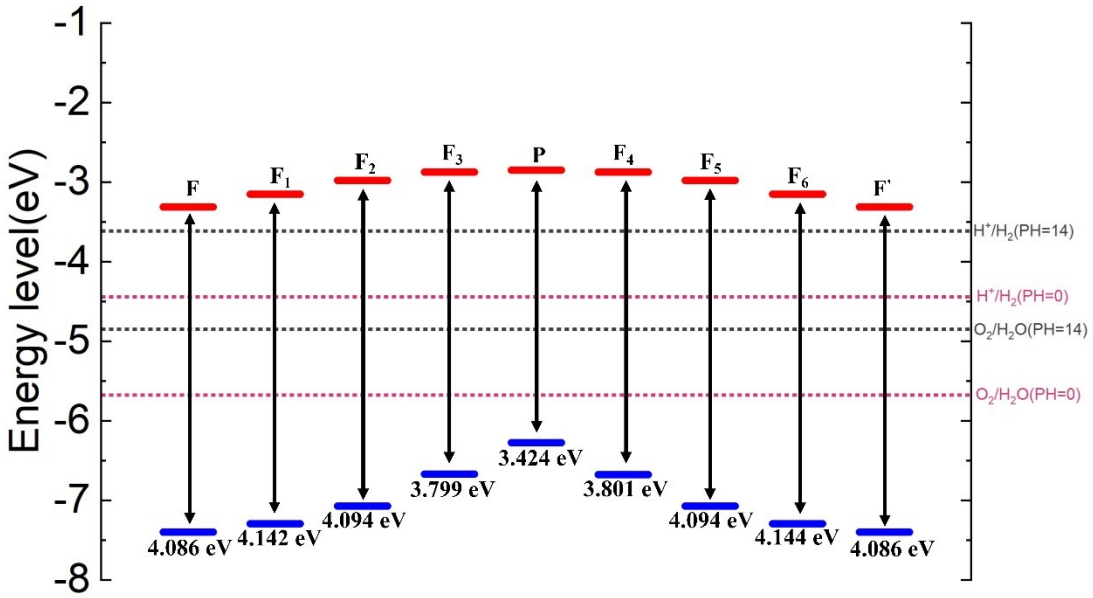

Fig. S11. Band-edge positions of different states of LuSCl monolayer during FE switching, shown in relation to the redox potentials of water, calculated using the HSE06 functional. The vacuum energy level is set to 0 eV. Intermediate states labeled F1 to F6 correspond to those identified in Fig. 4d.

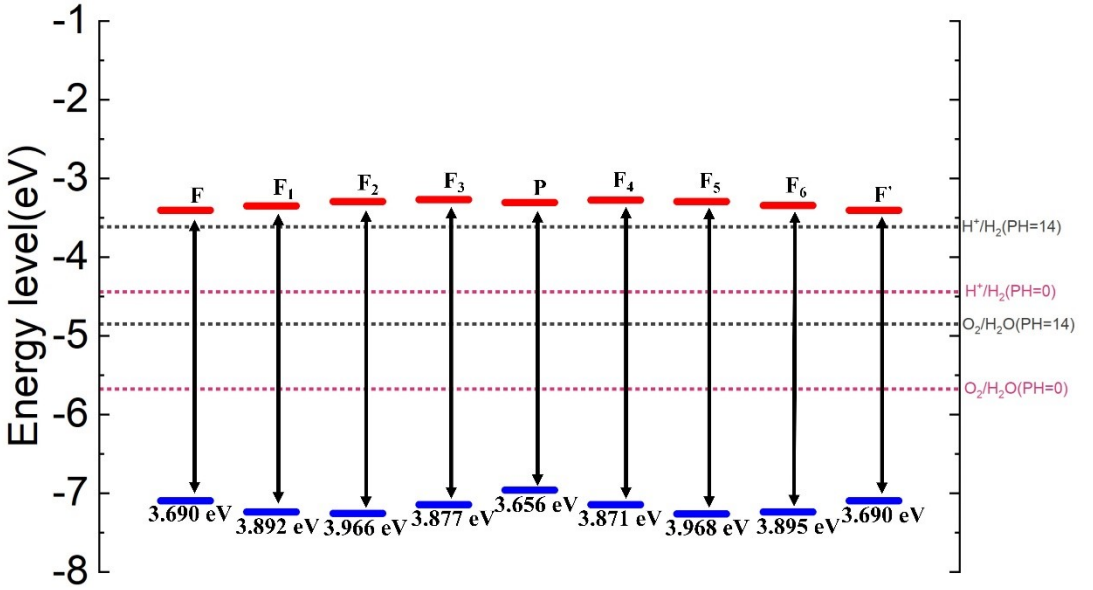

Fig. S12. Band-edge positions of different states of LuSI monolayer during FE switching, shown in relation to the redox potentials of water, calculated using the HSE06 functional. The vacuum energy level is set to 0 eV. Intermediate states labeled F1 to F6 correspond to those identified in Fig. 4d.

Table S1 Electron loss (-) and gain (+) occur for different atoms in LuSX (X=Br, Cl, I).

System	LuSBr	LuSCl	LuSI
Lu	-1.85e	-1.87e	-1.80e
S	+1.21e	+1.19e	+1.21e
X	+0.64e	+0.68e	+0.59e

Table S2. Elastic constants (in GPa) of LuSX monolayers.

Phase	**C_{11}**	**C_{22}**	**C_{12}**	**C_{44}**
LuSBr	21.527	29.804	0.845	7.976
LuSI	27.665	40.504	11.08	7.918
LuSCl	26.57	50.568	13.005	7.9

Table S3. CBM and VBM energies (in eV), photo-generated electrons/holes potentials (U_e and U_h), and redox potentials of water splitting ($U_{(H+/H)}$ and $U_{(O2/H2O)}$, in eV) at pH = 0, 7, and 14 for LuSX monolayers.

Energy levels	**LuSBr**	**LuSCl**	**LuSI**
CBM	-3.44	-3.31	-3.40
$U_{(H+/H)}$ at pH=0	-4.44	-4.44	-4.44
U_e at pH=0	1.0	1.13	1.04
$U_{(H+/H)}$ at pH=7	-4.027	-4.027	-4.027
U_e at pH=7	0.587	0.717	0.627
$U_{(H+/H)}$ at pH=14	-3.614	-3.614	-3.614
U_e at pH=14	0.174	0.304	0.214
VBM	-7.49	-7.40	-7.09
$U(O_2/H_2O)$ at pH=0	-5.67	-5.67	-5.67
U_h at pH=0	1.82	1.73	1.42
$U_{(O2/H2O)}$ at pH=7	-5.257	-5.257	-5.257

U_h at pH=7	2.233	2.143	1.833
$U_{(O2/H2O)}$ at pH=14	-4.844	-4.844	-4.844
U_h at pH=14	2.646	2.556	2.246